2.B: 2.G

Nuclear Physics **A327** (1979) 419–438;

THE SEPARATION OF PROTON AND DEUTERON SPIN-DEPENDENT EFFECTS IN THE ^{116}Sn(d, p)^{117}Sn REACTION

R. R. CADMUS, Jr. † and W. HAEBERLI

University of Wisconsin, Madison, Wisconsin 53706 ††

Received 14 March 1979

Abstract: The cross section, vector analyzing power, and proton polarization have been measured for the $l_n = 0$ reaction ^{116}Sn(d, p)^{117}Sn(g.s.) at 8.22 MeV. In addition, cross section and analyzing power data have been obtained at 8.22 MeV for ^{116}Sn($\vec{d}$, d)^{116}Sn and for ^{116}Sn(d, p)^{117}Sn leading to excited states of ^{117}Sn at 0.159, 0.317, 1.020, 1.179, 1.308 and 1.497 MeV. The cross section and analyzing power for ^{117}Sn($\vec{p}$, p)^{117}Sn and for ^{117}Sn($\vec{p}$, d)^{116}Sn leading to the 1.294 MeV state of ^{116}Sn have also been measured at 12.91 MeV. The data for ^{116}Sn(d, p)^{117}Sn(g.s.) have been used to separate the contributions to the analyzing power arising from spin-dependent forces in the proton and deuteron channels. A similar analysis is presented for an $l_n = 0$ ^{90}Zr(d, p)^{91}Zr transition at 11 MeV. Optical-model analyses have been performed for the elastic scattering data. The reaction data have been compared with distorted-wave calculations in order to investigate the validity of various deuteron potentials, as well as to extract spectroscopic information.

E

NUCLEAR REACTION ^{116}Sn($\vec{d}$, d), E = 8.22 MeV, measured $iT_{11}(\theta)$, $\sigma(\theta)$. ^{117}Sn($\vec{p}$, p), E = 12.91 MeV, measured $A_y(\theta)$, $\sigma(\theta)$. Deduced optical-model parameters. ^{116}Sn($\vec{d}$, p), E = 8.22 MeV, measured $iT_{11}(E_p, \theta)$, $\sigma(E_p, \theta)$, ^{117}Sn($\vec{p}$, d), E = 12.91 MeV, measured $A_y(E_d, \theta)$, $\sigma(E_d, \theta)$. Enriched targets.

1. Introduction

The usefulness of the distorted-wave Born approximation (DWBA) for the description of transfer reactions has been demonstrated many times for a wide variety of transitions and a wide range of energies. Frequently, however, polarization observables such as the vector analyzing power are poorly reproduced by the DWBA [ref. [1]].

It is important to understand the nature of such shortcomings because the DWBA plays a central role in a great deal of current theoretical and experimental work. In particular, reliable DWBA calculations are essential to the extraction of spectroscopic factors and orbital angular momentum transfers from cross-section measurements, and total angular momenta of final nuclear states from measurements of the vector analyzing power.

† Present address: Physics Department, Grinnell College, Grinnell, Iowa 50112.

†† Work supported in part by the US Energy Research and Development Administration.

It would clearly be desirable to separate the limitations of the basic theory from the inadequacies of the particular parameter sets which are used to describe the distorting potentials. This task would be greatly simplified if observables could be found which are independent of some of the terms in the optical potentials. The term that is of particular interest in distorted-wave calculations of the polarization and analyzing power in $l_n = 0$ (d, p) reactions is the spin-orbit term which appears in both the proton and deuteron channels. If the D-state of the deuteron is neglected, polarization effects in $l_n = 0$ transfers can only arise from spin-dependence in the optical potentials [2-4]). This is in contrast to the situation for higher values of l_n, for which polarization effects originate primarily with the central potentials [5,6]). Although the analyzing power and proton polarization for an $l_n = 0$ (d, p) reaction depend on both the proton and deuteron spin orbit potentials, Johnson has proposed a method [7]) which permits the separation of the spin-dependent effects in the two channels. Such a separation might make it possible to determine whether difficulties in describing polarization data for $l_n = 0$ transfers arise primarily from one spin-orbit potential or the other.

In Johnson's method, which is valid to first order in the spin-orbit potentials and is applicable only to $l_n = 0$ transfers, the analyzing power (A_y or iT_{11}) and polarization p_y are combined to form the quantities:

$$\begin{aligned} s_p &= 2(p_y - A_y) = 2p_y - 4\sqrt{\tfrac{1}{3}}iT_{11}, \\ s_d &= 3A_y - 2p_y = 2\sqrt{3}iT_{11} - 2p_y. \end{aligned} \tag{1}$$

Here A_y and iT_{11} are the vector analyzing powers in Cartesian and spherical coordinates, respectively. The linear combinations s_p and s_d have the property that each is proportional to the spin-orbit potential for the particle denoted by the subscript, and is independent of the other spin-orbit potential. With these definitions, s_p can be interpreted as the Cartesian analyzing power arising from the proton spin dependence only, and s_d can be interpreted as the Cartesian analyzing power arising from the deuteron spin dependence only. Eqs. (1) are valid only if the analyzing power and polarization are unaffected by the D-state of the deuteron. As shown in ref. [4]), the D-state does have a substantial effect, but the spin-dependent effects in the two channels are still separated by constructing s_p and s_d for the case of interest here. Ref. [4]) also contains a more complete discussion of the properties of s_p and s_d.

In this paper we present the results of the first experimental determination of s_p and s_d. The measurements were made for the $l_n = 0$ transition ^{116}Sn(d, p)^{117}Sn (g.s.) at an energy of 8.22 MeV. The details of the experimental method, as well as the reasons behind the choice of this reaction, are discussed in the next section. As described in sect. 3, we have used these data in an attempt to isolate the contributions to these quantities from the proton and deuteron channels using Johnson's method in order to clarify the roles played by the corresponding optical potentials. We have

also applied this technique to the case of an $l_n = 0$ ^{90}Zr(d, p)^{91}Zr transition using the data of refs. [8,9]). In order to obtain the appropriate phenomenological optical potentials for use in distorted-wave calculations for ^{116}Sn(d, p)^{117}Sn, we have also measured the cross section and vector analyzing power for the elastic scattering of deuterons from ^{116}Sn at 8.22 MeV and the elastic scattering of protons from ^{117}Sn at 12.91 MeV, which is the energy of the outgoing protons in the ^{116}Sn(d, p)^{117}Sn (g.s.) reaction. The elastic scattering data and the associated optical model analysis are presented in sect. 4. The results of the DWBA analysis of the ^{116}Sn(d, p)^{117}Sn (g.s.) measurements are described in sect. 5.

In the process of measuring σ, iT_{11}, and p_y for the ^{116}Sn(d, p)^{117}Sn(g.s.) reaction, we also studied a number of other transitions in this reaction at 8.22 MeV, and in the ^{117}Sn($\vec{p}$, d)^{116}Sn reaction at 12.91 MeV. The spectroscopic information which was extracted from these measurements is discussed in sect. 6. In addition, these data were compared to DWBA calculations in order to investigate the validity of the traditional DWBA method. In particular, we have compared the results obtained using phenomenological optical potentials in the standard DWBA with results obtained using the adiabatic prescription of Johnson and Soper [10]), in which breakup effects are taken into account. This comparison is described in sect. 7. The conclusions reached in this series of experiments are summarized in sect. 8.

2. Experimental method

Johnson's method [7]) for separating proton and deuteron spin-dependent effects requires measurements of both the analyzing power and proton polarization for an $l_n = 0$ reaction. The analyzing power is easily obtained by measuring the asymmetry of the outgoing protons when the reaction is initiated by a polarized deuteron beam. The easiest way to obtain the proton polarization, however, is not a direct measurement, but a measurement of the analyzing power in the inverse reaction using a polarized proton beam. This approach yields the required polarization data, since the polarization in the (d, $\vec{p}$) reaction is equal to the analyzing power in the inverse ($\vec{p}$, d) reaction [11,12]).

The use of the inverse reaction to obtain the proton polarization p_y severely limits the choice of target nuclei because one requires that an $l_n = 0$ neutron transfer connect the ground states of two adjacent stable isotopes. The ^{116}Sn(d, p)^{117}Sn(g.s.) reaction is one of the few cases in which this condition is met. Light nuclei ($A \lesssim 30$) are undesirable candidates because of the effects of compound nucleus formation.

In the first part of the experiment, a 12.91 MeV polarized proton beam was used to measure the cross section and analyzing power for ^{117}Sn($\vec{p}$, d)^{116}Sn(g.s.) (the inverse reaction). The same quantities were simultaneously measured for ^{117}Sn($\vec{p}$, p)^{117}Sn. In the second part of the experiment, an 8.22 MeV polarized deuteron beam was employed to determine the cross section and vector analyzing power for ^{116}Sn($\vec{d}$, p)^{117}Sn(g.s.) and ^{116}Sn($\vec{d}$, d)^{116}Sn. The bombarding energies satisfy the

requirement that the c.m. energy be the same in the two reactions. Analysis of the proton and deuteron elastic scattering data provides optical potentials for the nuclei and energies which are appropriate for DWBA analysis of the reaction data. In both the ($\vec{d}$, p) and ($\vec{p}$, d) experiments the cross sections and vector analyzing powers for transitions to excited states were also measured.

The technique used to determine the cross sections and analyzing powers in both the proton and deuteron-beam experiment was the same. A vector-polarized proton or deuteron beam was produced by the Wisconsin Lamb-shift polarized-ion source [13]) and tandem accelerator. The targets were self-supporting metallic foils 1.5 mg/cm^2 thick (or 0.8 mg/cm^2 for forward angle data) for ^{116}Sn and 3.13 mg/cm^2 for ^{117}Sn. The ^{116}Sn and ^{117}Sn targets were 96% and 89% enriched, respectively. The outgoing protons and deuterons were detected by an array of four solid state detector telescopes on the left side of the beam. Detector telescopes were used to allow particle identification [14]). The detectors were 9.4 cm from the target and subtended 4.9 msr. The angular acceptances of the detectors were approximately $\pm 1°$. The detector positions were chosen to correspond to the same c.m. angles in the ($\vec{d}$, p) and ($\vec{p}$, d) ground state measurements. The method of ref. [15]) was used to correct for dead time in the electronics. Pileup rejection was employed for measurements at the most forward angles.

The polarization of the deuteron beam was determined using a d-^{4}He polarimeter [ref. [16])] located at the rear of the scattering chamber. The polarization of the proton beam was measured in a similar fashion, using a p-^{4}He polarimeter [17]). The analyzing power of this polarimeter was measured by comparing the left-right asymmetry in the polarimeter with that in a simultaneous good-geometry ^{4}He(p, p) ^{4}He experiment at a lab scattering angle of 111.5°. The p-^{4}He analyzing power

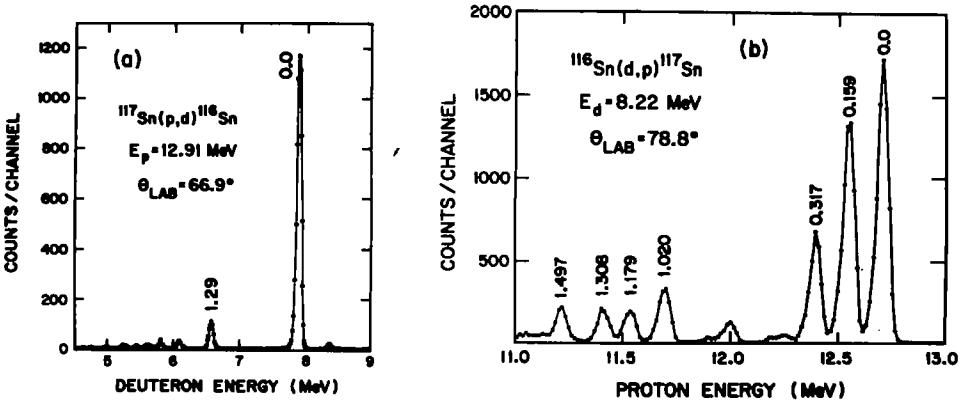

Fig. 1a. A representative pulse-height spectrum for the ^{117}Sn(p, d)^{116}Sn reaction at $\theta_{lab} = 66.9°$.

Fig. 1b. A representative pulse-height spectrum for the ^{116}Sn(d, p)^{117}Sn reaction at $\theta_{lab} = 78.8°$. In both spectra the transitions studied in this paper are labelled with the energies of the corresponding states in the residual nuclei.

at this angle and energy was calculated from the phase shifts of ref. [18]), and is very close to the maximum possible value. The deuteron beam polarization it_{11} was generally about 0.50, while the proton beam polarization p_y was typically 0.75.

The product of the number of incident particles times the target thickness for each run was determined using monitor detectors [14,19]) which detected elastically scattered particles at 13.1° on opposite sides of the beam. The cross sections for scattering at this angle were calculated from an optical model, but the results are extremely insensitive to the choice of parameters because the cross sections are very close to the Rutherford values in these cases. For the measurements with the deuteron beam, unpolarized runs were taken in addition to the normal "spin up" and "spin down" runs in order to permit the detection of tensor effects as explained below.

A typical ^{117}Sn(p, d)^{116}Sn pulse-height spectrum (fig. 1a) shows that the ground state peak is completely isolated. In the ^{116}Sn(d, p)^{117}Sn spectra, however, the peaks of interest overlap slightly with their neighbors, as shown in fig. 1b. In this case the number of counts in each peak was determined using a peak-fitting procedure.

The cross section and vector analyzing power were obtained from the number of counts for each transition using the method of ref. [20]). For deuterons this method is subject to error if the deuteron beam has a tensor component. The analyzing powers for the (d⃗, d) and (d⃗, p) experiments were therefore redetermined using [19,21])

$$iT_{11} = \frac{1}{4it_{11}}\left(\frac{Y_\uparrow - Y_\downarrow}{Y_0}\right), \tag{2}$$

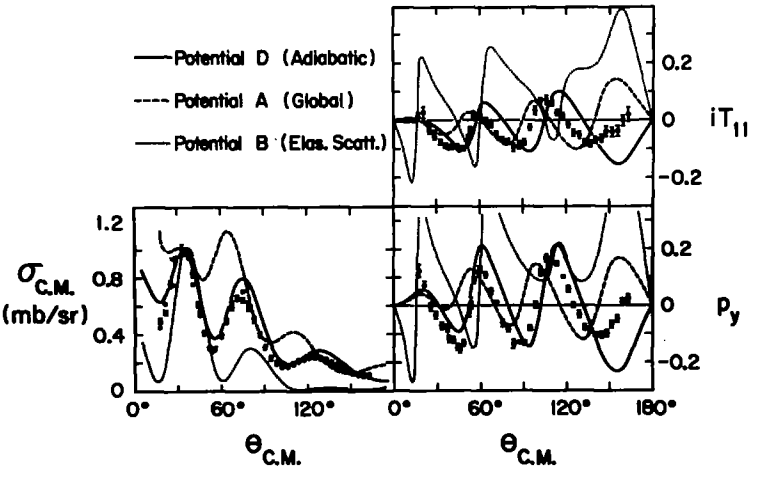

Fig. 2. Cross section, vector analyzing power, and proton polarization data for the ^{116}Sn(d, p)^{117}Sn(g.s.) reaction. The cross section data represented by the closed symbols were obtained directly from observations of the (d, p) reaction, while those represented by the open symbols were obtained from the (p, d) measurements and renormalized as explained in the text. The curves are the results of distorted-wave calculations using different deuteron optical potentials.

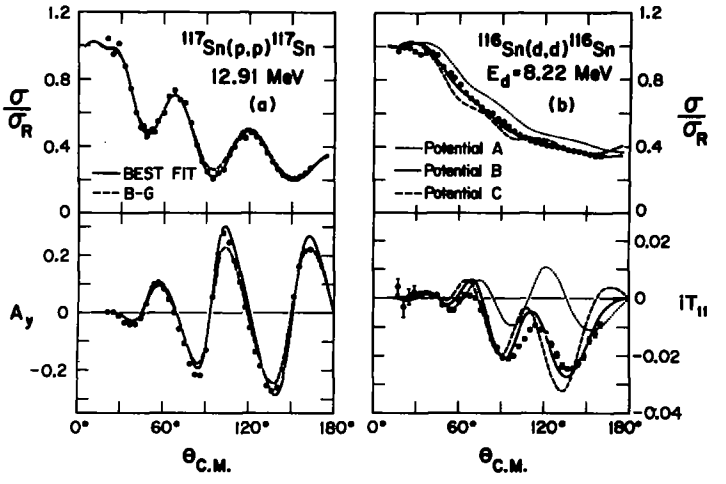

Fig. 3a. Cross section and analyzing power for ^{117}Sn(p⃗, p)^{117}Sn at 12.91 MeV. The curves are optical-model calculations using the potential which best fit the data (solid curve) and the potential of Becchetti and Greenlees [28]) (broken curve).

Fig. 3b. Cross section and vector analyzing power for ^{116}Sn(d⃗, d)^{116}Sn at 8.22 MeV. The curves are optical-model calculations using the potentials shown.

where it_{11} is the vector polarization of the beam, and $Y_\uparrow$, $Y_\downarrow$, and Y_0 are the ratios of the numbers of counts from the transition of interest to the number of counts observed in the two monitor detectors for the spin-up, spin-down, and unpolarized runs. This method is independent of a tensor component in the beam, and gave analyzing powers which agreed within the uncertainties involved with those obtained using the method of ref. [20]). Therefore, the uncertainty from a possible tensor polarization of the deuteron beam is negligible. The results were corrected for dead time in the electronics, enrichment of the target, target contamination and the finite size of the detectors.

The error bars shown with the measurements in figs. 2 and 3 indicate the size of the uncertainties arising from counting statistics, peak summation, statistical effects in the determination of the beam polarizations, and uncertainties in the detector solid angles and angle settings. In addition, the overall normalizations of the analyzing power measurements are subject to uncertainties of $\pm 1\%$ for the (p, p) and (p, d) data, and $\pm 5\%$ for the (d, d) and (d, p) data because of the uncertainties in the polarimeter calibrations. Known uncertainties affecting the overall normalization of the cross section data lead to estimated normalization uncertainties of $\pm 3\%$ for the (p, p) and (p, d) data and $\pm 2\%$ for the (d, d) and (d, p) data. However, the (d, p) and (p, d) ground state cross sections must be identical except for a factor which can be calculated from the principle of detailed balance. For the present measurements the ratio of the (d, p) cross sections to the (p, d) cross sections was 10% larger than the detailed balance value, so the (p, d) and (p, p) cross sections were adjusted upward

by 5%, while the (d, p) and (d, d) cross sections were adjusted downward by the same amount. The resulting (d, p) and (p, d) ground state cross sections are in excellent agreement over the entire angular range, as shown by the open and closed symbols in fig. 2, but the normalizations of the cross sections are evidently more uncertain than estimated above. However, the forward angle behavior of the (p, p) and (d, d) cross section data (fig. 3) indicate that the normalizations are not in error by more than about $\pm 5\%$.

3. Proton and deuteron contributions to the analyzing power and proton polarization

The results for the ^{116}Sn(d, p)^{117}Sn ground state transition are shown in fig. 2. The open symbols show the cross sections for ^{117}Sn(p, d)^{116}Sn, multiplied by a factor of 1.065 (calculated from the principle of detailed balance) to permit direct comparison with the ^{116}Sn(d, p)^{117}Sn cross section measurements. The angular dependence of the cross section is characteristic of a direct reaction. The two panels on the right side of fig. 2 display the vector analyzing power and proton polarization for ^{116}Sn(d, p)^{117}Sn(g.s.). As explained in sect. 2, the measurements of p_y made use of the inverse reaction.

The values of s_p and s_d calculated from the experimental values of p_y and iT_{11} according to eqs. (1) are shown in fig. 4. The quantities s_p and s_d are comparable in magnitude, indicating that proton and deuteron spin-orbit interactions contribute to iT_{11} in approximately equal amounts. Fig. 4 also shows that s_p and s_d are opposite in sign at most angles, and both quantities are roughly twice as large in absolute magnitude as iT_{11}. This result reveals that the analyzing power is the result of substantial cancellation of the effects resulting from the proton and deuteron spin-orbit

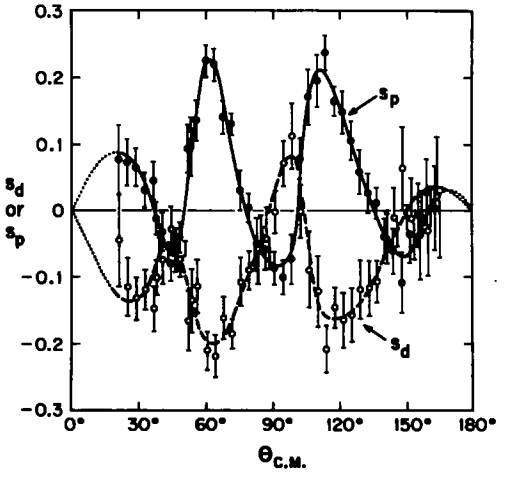

Fig. 4. Angular distributions of s_p and s_d obtained from the analyzing power and proton polarization measurements shown in fig. 2. Smooth curves have been drawn through the data.

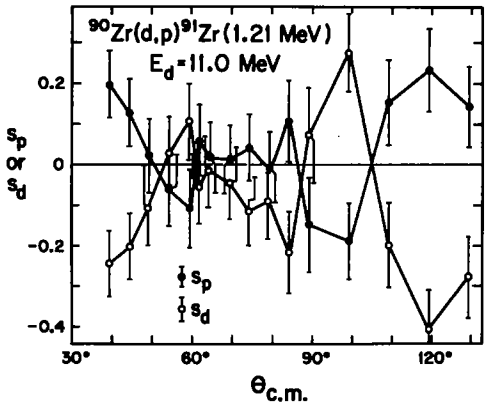

Fig. 5. Angular distributions of s_p and s_d for ^{90}Zr(d, p)^{91}Zr (E_x = 1.201 MeV) at 11 MeV. These results were obtained from the analyzing power data of ref. [8]) and the proton polarization data of ref. [9]) as explained in the text. Neighboring data points have been connected with straight lines for clarity.

terms. This second observation explains, to some extent at least, the difficulty often experienced in fitting the analyzing power for $l_n = 0$ (d, p) reactions, because errors in the calculated effects due to the proton and deuteron spin-orbit potentials will be magnified if the two effects tend to cancel.

Johnson's method [7]) can also be applied to the case of the ^{90}Zr(d, p)^{91}Zr reaction leading to the first excited state in ^{91}Zr. The analyzing power for this $l_n = 0$ transfer has been measured by Rathmell *et al.* [8]) at 11 MeV, and the polarization of the outgoing protons has been determined directly by Michelman *et al.* [9]), also at a deuteron energy of 11 MeV. Since the measurements were not made at the same reaction angles in these two experiments, a smooth curve was drawn through the analyzing power data, and values were read off for the angles at which polarization data were available. The angular distributions of s_p and s_d obtained from eq. (1) are shown in fig. 5. Again, s_p and s_d tend to be opposite in sign, and of roughly equal magnitude, as was the case for the ^{116}Sn(d, p)^{117}Sn results. Earlier workers [22,23]) had claimed that proton spin-dependent effects were dominant, but no such dominance is evident in the cases examined here.

4. Results and optical-model analysis for elastic scattering

The measured cross sections and vector analyzing powers for ^{117}Sn($\vec{p}$, p)^{117}Sn and ^{116}Sn($\vec{d}$, d)^{116}Sn are shown in fig. 3. The proton elastic scattering data show the usual oscillations in the cross section, and large oscillations about zero in the analyzing power. For ^{116}Sn($\vec{d}$, d)^{116}Sn, on the other hand, the cross section falls monotonically with angle, and the vector analyzing power is not only very small, but also predominantly negative. This behavior has been observed in a number of other cases involving the scattering of deuterons with $E_d \lesssim 12$ MeV from nuclei with $A > 100$

[refs. [14,24-26])]. It is interesting to note that the "derivative rule" [27]) applied to the (d, d) cross section predicts a predominantly negative analyzing power.

The results for elastic scattering were analyzed in terms of a standard optical model using a potential of the form given in refs. [19,28]). The calculations were performed using the code SNOOPY-2 [ref. [29])]. A Coulomb radius parameter of 1.22 fm was used for all calculations.

The ^{117}Sn($\vec{p}$, p)^{117}Sn data are described fairly well by the global proton potential of Bechetti and Greenlees [28]) as shown by the dashed curves in fig. 3a, but a slight adjustment of the parameters produced a noticeably better fit to the data (solid curves in fig. 3a). The parameters of these potentials are given in table 1. The ^{116}Sn($\vec{d}$, d)^{116}Sn data were considerably more difficult to fit, primarily because the vector analyzing power is predominantly negative, and a great deal of effort was expended in the search for a potential which reproduced this feature of the data. Calculations were performed using published potentials [25,30-32]), and parameter searches were made using these potentials as starting points. Searches were also made starting with parameter sets which had been obtained by minor modifications of published potentials. No acceptable fits were obtained in this way. An example of the problems encountered is shown by the dotted curves in fig. 3b. These calculations,

TABLE 1

Proton and deuteron optical model parameters [a])

Particle	Potential	V	r_0	a_0	w_S	w_D	r_w	a_w	$V_{s.o.}$	$r_{s.o.}$	$a_{s.o.}$
p	BG (ref. [29]))	57.45	1.17	0.75	0.14	10.32	1.32	0.61	6.20	1.01	0.75
p	best-fit	58.17	1.17	0.73	0.26	8.53	1.28	0.68	6.19	1.00	0.78
d	A (global [25]))	113.68	1.05	0.86	0.0	9.17	1.43	0.81	7.00	0.75	0.50
d	B (from (d, d))	139.52	1.02	0.56	0.0	4.59	1.81	0.80	5.69	0.98	1.00
d	C (from (d, d))	111.30	1.10	0.85	0.0	5.26	1.92	0.72	5.69	0.98	1.00
d	D (adiabatic)	114.07	1.17	0.79	0.0	22.40	1.26	0.62	6.20	1.01	0.75

[a]) The potential parameters are defined as in ref. [28]), except that for deuterons (spin 1) the product $\boldsymbol{l} \cdot \boldsymbol{\sigma}$ was replaced by $\boldsymbol{l} \cdot \boldsymbol{s}_d$, where $\boldsymbol{s}_d$ is the deuteron spin operator ($|\boldsymbol{s}_d|^2 = 2$). Potential depths are given in MeV; geometrical parameters are given in fm.

performed with the global potential of Lohr and Haeberli [25]) (A in table 1), without any adjustment of parameters, overestimate the cross section over most of the angular range, and fail to reproduce the negative trend of the analyzing power.

Following the failure of published potentials to lead to acceptable fits to the (d, d) data, searches were made with initial values of the parameters of the central potential which differed significantly from published parameters. For these calculations the parameters of the spin-orbit potential were those calculated from the folding model [33]) for ^{120}Sn [ref. [32])]. The central potentials obtained from the folding model have been shown [34]) to require substantial adjustment to obtain

agreement with experimental data. The solid curves in fig. 3b represent the best fit obtained with the folding model spin-orbit potential. The parameters of the central potential were adjusted to reproduce the data. The cross section and analyzing power are both reproduced fairly well, but the corresponding potential (B in table 1) has a real central term which is abnormally deep and has an unreasonably small diffuseness compared with a potential obtained by adding proton and neutron potentials. The potential labelled C in table 1 is the result of an attempt to obtain more conventional values of V and a_0, while retaining a reasonably good fit to the data. These parameters were obtained by repeatedly lowering V and increasing a_0, while simultaneously readjusting the remaining parameters of the central potential. The best fit obtainable became steadily worse as a_0 was increased. Potential C still reproduces the general features of the data (dashed curves in fig. 3b), but the agreement with both σ and iT_{11} is considerably worse than was obtained with potential B. The increase in a_0 was responsible for about half of the degradation in the fit to iT_{11}, and all of the degradation in σ. The lower value of V caused the remaining degradation in the fit to iT_{11}.

In order to determine whether the difficulties encountered in fitting the data were caused by the neglect of tensor potentials in the analysis above, additional calculations were performed with a potential containing a tensor term. The calculations were done using the code DD [ref. [35])] and employed optical potential B to which was added a tensor term of the T_R [ref. [36])] variety calculated from the folding model [32,33]). The inclusion of the T_R potential had only a very slight effect on the calculations.

The best choice of a deuteron potential for use in DWBA calculations is therefore unclear. Although a large number of searches was performed (only a few of which have been described here), and a large volume of parameter space was explored, this effort led to the conclusion that a reasonably good fit to the (d, d) data can only be obtained with unconventional values of V and a_0. Difficulty in fitting predominantly negative analyzing powers has been reported in other cases [24-26]), and it has been suggested [37]) that the difficulty is related to the fact that the deuteron energy is near, or only slightly above, the Coulomb barrier in these cases. However, our calculations are insensitive to reasonable changes in the radius of the charge distribution, so it seems unlikely that the problem is simply due to an incorrect description of the Coulomb potential.

5. DWBA analysis of the ^{116}Sn(d, p)^{117}Sn(g.s.) data

In the standard DWBA procedure, the optical potentials which are used to calculate the incoming and outgoing distorted waves in a (d, p) reaction are the same potentials which describe the elastic scattering of deuterons and protons from the target and residual nuclei, respectively. The elastic scattering data which are used to obtain the potentials must, of course, be taken at the c.m. energies of the incoming and outgoing

particles in the (d, p) reaction. The data presented in sect. 4 meet these requirements, and DWBA calculations using the optical potentials obtained by fitting these data would therefore by expected to lead to reasonable fits to the data for ^{116}Sn(d, p)^{117}Sn described in sect. 3.

Distorted-wave calculations for the (d, p) reaction were performed using the code DWCODE [ref. [38])]. These calculations included the effects of the deuteron D-state [39]), as well as corrections for the finite range of the n-p interaction †. The finite range parameter was taken to be $\beta = 1.334$ fm^{-1} [ref. [39])]. A Coulomb radius parameter of 1.22 fm and the "best-fit" proton potential were used for all (d, p) calculations discussed in this paper. The results of calculations using deuteron potential B are shown as the dotted curves in fig. 2. These calculations fail to reproduce the data even qualitatively. Similar calculations using deuteron potential C resulted in even worse fits. The failure of these calculations to reproduce the reaction data indicates that potentials which describe the elastic scattering data are not necessarily appropriate for use in the DWBA. This will be discussed at greater length in sect. 7.

Because earlier work has determined the proton-nucleus potential better than the deuteron-nucleus potential, and because the ^{116}Sn(d, d)^{116}Sn data obtained in this experiment are qualitatively different from those obtained at deuteron energies well above the Coulomb barrier, a natural starting point for further attempts to reproduce the (d, p) data is the investigation of other deuteron potentials. The dashed curves in fig. 2 were calculated using deuteron potential A. The fits to iT_{11} and p_y are much better than those obtained with potential B, but the fit to the cross section is still poor. The global deuteron potential of Perey and Perey (potential A of ref. [40])) was also tried, and was successful in some respects, but did not lead to strikingly improved fits to all the data.

Calculations were also done using a deuteron potential obtained from the adiabatic prescription of Johnson and Soper [10,41]). This approach is similar to the folding model of Watanabe [33]), except that the sum of the proton-nucleus and neutron-nucleus potentials is multiplied by the neutron-proton interaction before being averaged over the internal wave function of the deuteron. This approach represents an extension of the DWBA method because the effects of deuteron breakup on the neutron transfer have been taken into account. The neutron and proton potentials to be used in this procedure must be taken at an energy equal to half the energy of the incident deuteron in the (d, p) reaction, or about 4.1 MeV in the present case. The neutron potential used in constructing the adiabatic deuteron potential was taken directly from the neutron potential of Becchetti and Greenlees [28]), and is based primarily on data at energies below 10 MeV. The proton potential of ref. [28]) was not used directly because the proton scattering data analyzed in that work were

† After this paper was completed, Dr. R. C. Johnson of the University of Surrey reported to us the discovery by J. A. Tostevin of an error in DWCODE. The calculations presented in this paper were repeated after correction of the error, and only minor discrepancies with the original calculations were found. None of the conclusions of this paper are affected.

all obtained at energies above 10 MeV, so that a considerable extrapolation is required to obtain a proton potential at 4.1 MeV. For the calculations which follow, the proton potential for Sn at 4.1 MeV was obtained from the neutron potential of ref. [28]) by reversing the sign of the asymmetry terms in the real and imaginary central potentials, and adding to the real central potential the $Z/A^{\frac{1}{3}}$ term which is present for protons. The parameters of the adiabatic potential are given in table 1 as potential

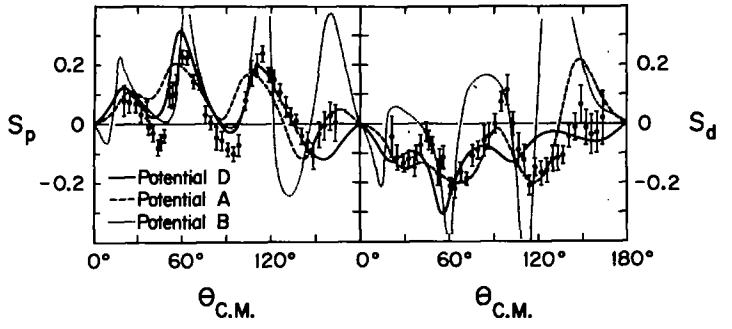

Fig. 6. Distorted-wave calculations for s_p and s_d using various deuteron potentials. The data are those of fig. 4.

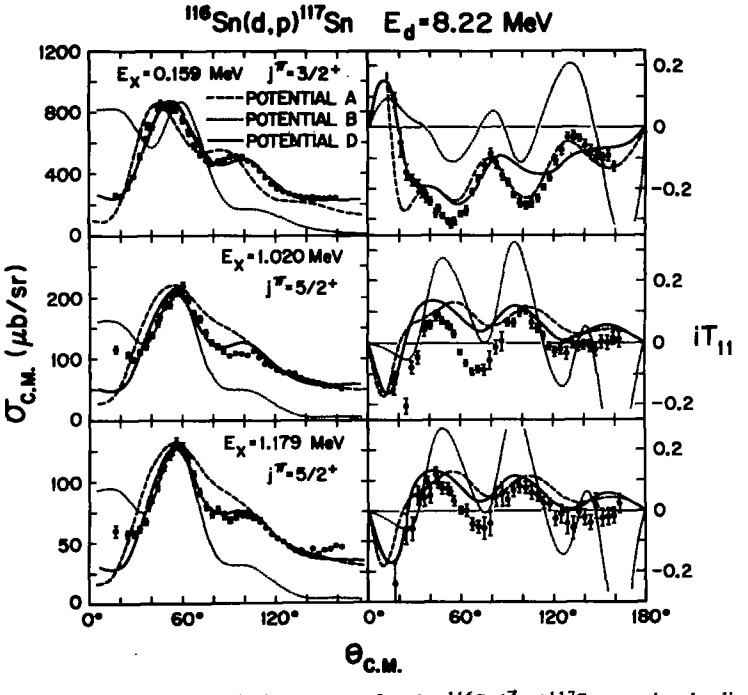

Fig. 7. Cross sections and vector analyzing powers for the ^{116}Sn(d⃗, p)^{117}Sn reaction leading to states in ^{117}Sn at 0.159, 1.020, and 1.179 MeV. These are all $l_n = 2$ transitions. The curves are the results of distorted-wave calculations which do not include the effects of the D-state of the deuteron.

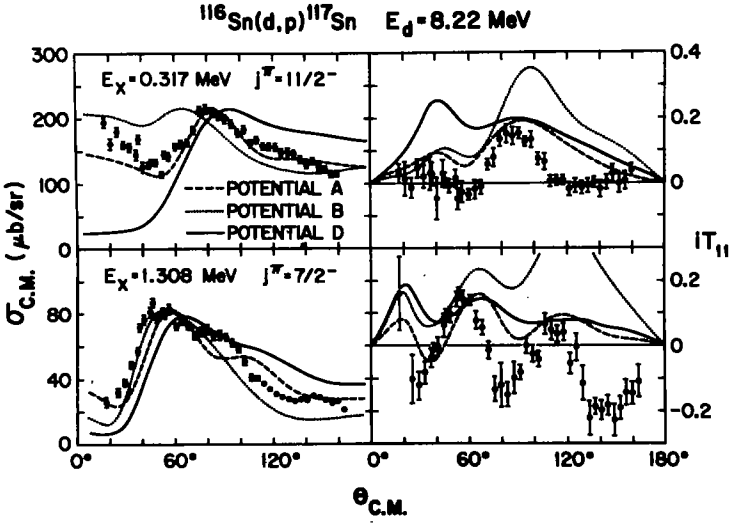

Fig. 8. Cross sections and vector analyzing powers for the ^{116}Sn(d, p)^{117}Sn reaction leading to states in ^{117}Sn at 0.317 MeV (l_n = 5) and 1.308 MeV (l_n = 3). The curves are the results of distorted-wave calculations which do not include the effects of the D-state of the deuteron.

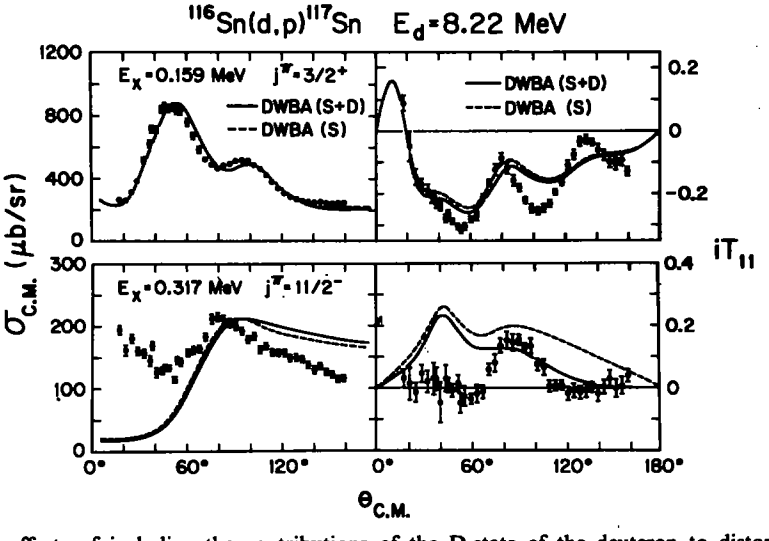

Fig. 9. The effects of including the contributions of the D-state of the deuteron to distorted-wave calculations for the (d, p) transitions to states in ^{117}Sn at 0.159 and 0.317 MeV. These cases represent the least and greatest effects observed for any of the transitions studied in this paper. The same spectroscopic factor was used in both calculations for each transition. The solid curves include both S- and D-state contributions, while the broken curves include only the S-state contribution.

D. The calculations done with the adiabatic deuteron potential (solid curves in fig. 2) reproduce the reaction data better than do the calculations done with potentials A or B. Further calculations using these potentials will be discussed in sect. 7.

A comparison of DWBA calculations for s_p and s_d with the measured angular distributions for these quantities offers the possibility of learning whether discrepancies between theory and experiment can be attributed to the inadequacy of either the proton or the deuteron spin-orbit potential or both. A better fit to s_p than to s_d, for example, would indicate that the difficulties arise from an incorrect deuteron spin-orbit potential.

The results of DWBA calculations for s_p and s_d using deuteron potentials A, B, and D are shown in fig. 6. The fits with potential B are poor, as would be expected from the poor fits to iT_{11} and p_y. The calculations with potentials A and D reproduce the main features of the data for s_p and s_d, but significant discrepancies remain. The fact that the calculations fail to reproduce the details of the measurements for both s_p and s_d indicates that the problem is not limited to an inappropriate spin-orbit potential in only one channel. An incorrect description of the central potentials, for example, could lead to poor fits to both s_p and s_d. However, as indicated in sect. 4, the proton potential is much better determined in the present case than is the deuteron potential, so it is likely that the lack of agreement between the measured and calculated angular distributions of s_p and s_d is the result of inadequacy of the deuteron central potential.

6. Transitions to excited states

In addition to the results for the ground state transitions, we have also obtained data for the ^{116}Sn($\vec{d}$, p)^{117}Sn and ^{117}Sn($\vec{p}$, d)^{116}Sn reactions leading to a number of excited states in ^{117}Sn and ^{116}Sn. The cross sections and vector analyzing powers for the (d, p) transitions leading to states in ^{117}Sn at 0.159, 0.317, 1.020, 1.179, and 1.308 MeV are shown in figs. 7–9. The excitation energies are those of Madueme *et al.*[42]). The analyzing power for the (d, p) transition to the 1.497 MeV state is shown in fig. 10. The cross section and analyzing power for the (p, d) reaction leading to the 1.294 MeV state in ^{116}Sn are displayed in fig. 11. Although the cross sections presented here are not large, the shapes of the angular distributions indicate that these transitions proceed primarily by direct reaction processes.

The DWBA calculations shown in figs. 7 and 8 were performed using the methods described in sect. 5. The D-state of the deuteron is neglected in these calculations, but the effect of the D-state for a single choice of deuteron potential is shown in fig. 9. The two examples shown represent the largest and smallest D-state effects observed for the five excited states of ^{117}Sn which were investigated in this experiment. The cross sections are essentially unaffected, but the analyzing power is shifted toward more negative values by an amount which increases with increasing l_n. The D-state effects are not large enough to alter the conclusions drawn from S-state calculations.

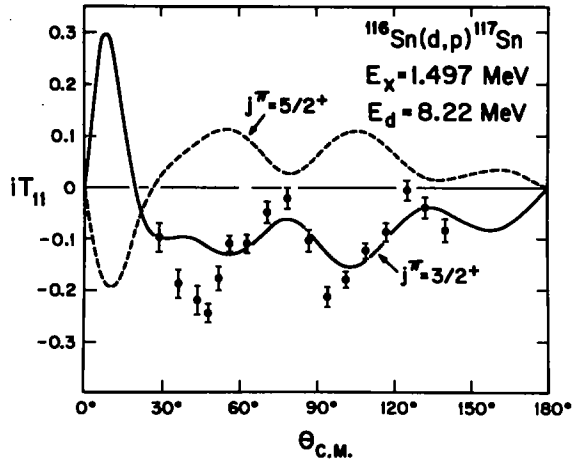

Fig. 10. Vector analyzing power for the ^{116}Sn(d, p)^{117}Sn reaction leading to the 1.497 MeV state in ^{117}Sn. Distorted-wave calculations are shown for the two choices of j^π which are consistent with $l_n = 2$.

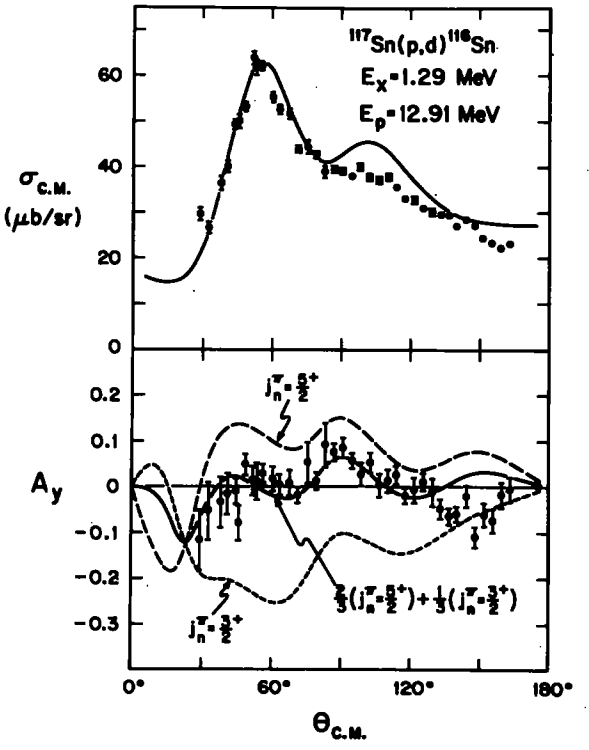

Fig. 11. Cross section and analyzing power for the ^{117}Sn(p, d)^{116}Sn transition to the 1.294 MeV state in ^{116}Sn. The curves are distorted-wave calculations done with deuteron potential D. The two dashed curves correspond to the two possible values of the toal angular momentum of the transferred neutron. The solid curve was obtained by assuming that the contribution to the reaction from $j_n^\pi = \frac{1}{2}^+$ is twice as large as that from $j_n^\pi = \frac{3}{2}^+$.

In figs. 7 and 8 calculations are shown only for the choices of j^π which lead to the best fits to the data. The spin and parity assignments for these states will be discussed later in this section. As was the case for the ground state transition, the use of the deuteron potentials obtained from analysis of the elastic scattering data (potentials B and C in table 1) does not lead to acceptable fits to the data. Calculations using the potential of ref. [25]) (potential A in table 1) or the adiabatic potential (potential D in table 1) are much more successful in reproducing the data, however. The adiabatic potential leads to better overall agreement with the data for the $l_n = 2$ transitions (fig. 7) than does the potential A, but the situation is reversed for the $l_n = 3$ and $l_n = 5$ transitions shown in fig. 8. The relative success of these three potentials will be duscussed at greater length in the next section.

The j-dependence of the vector analyzing power [6]) in (d, p) reactions is well established, and leads to reliable spin assignments. For the transitions included in figs. 7 and 8, the calculations shown reproduce the data much better than do calculations with the alternative choices for j^π, for which iT_{11} usually has the wrong sign. These results therefore confirm previous spin assignments [26,42–44]) to the 0.159, 0.317 and 1.179 MeV states. The existence of a $j^\pi = \frac{5}{2}^+$ state near 1.020 MeV [ref. [44])] is also confirmed. In the present experiment the previously reported $j^\pi = \frac{3}{2}^+$ state at 1.005 MeV [refs. [42,43])] would not be resolved from the 1.020 MeV state, but the $\frac{3}{2}^+$ state is evidently not strongly excited in the ^{116}Sn(d, p)^{117}Sn reaction at 8.22 MeV, since the present data for the 1.020 MeV state are nearly identical to those for the $j^\pi = \frac{5}{2}^+$ state at 1.179 MeV, and show no evidence of a contribution with the characteristics of the data for the $j^\pi = \frac{3}{2}^+$ state at 0.159 MeV. The vector analyzing power for the transition to the 1.497 MeV state in ^{117}Sn is shown in fig. 10. Although these data are of lower quality than those for the other transitions, the trend of the data is clear. This transition has been assigned $l_n = 2$ (refs. [44,45])), restricting the spin and parity of the final state to $j^\pi = \frac{3}{2}^+$ or $\frac{5}{2}^+$. The data shown in fig. 10 are compatible only with an assignment of $j^\pi = \frac{3}{2}^+$, not only because distorted-wave calculations using the adiabatic potential (potential D in table 1) yielded far better agreement with the measurements for this choice of spin, but also because the data for this transition are very similar to the analyzing power data for the transition leading to the $j^\pi = \frac{3}{2}^+$ state at 0.159 MeV. The present $j^\pi = \frac{3}{2}^+$ assignment is in conflict with a previous tentative $j^\pi = \frac{5}{2}^+$ assignment [44]).

In addition to the data for the ^{117}(p̄, d)^{116}Sn(g.s.) transition presented earlier in this paper, we have also measured the cross section and analyzing power for the (p, d) transition to the 1.294 MeV first excited state of ^{116}Sn. These data are shown in fig. 11. The curves in this figure are the results of DWBA calculations using the adiabatic deuteron potential (potential D in table 1). The effect of the deuteron D-state has not been included. The two broken curves in the lower half of the figure correspond to the only two values of the angular momentum of the transferred neutron which can contribute to a transition between the $j^\pi = \frac{1}{2}^+$ ground state of ^{117}Sn and the 1.294 MeV state in ^{116}Sn, which is known to have $j^\pi = 2^+$ [ref. [46])].

These two values are $j_n^\pi = \frac{3}{2}^+$ and $j_n^\pi = \frac{5}{2}^+$. Neither of these calculations fits the data particularly well, but a mixture of these two processes in which the $j_n^\pi = \frac{5}{2}^+$ transfer contributes twice as strongly as does the $j_n^\pi = \frac{3}{2}^+$ transfer gives a much improved fit, as shown by the solid curves in fig. 11. The calculated cross section is essentially identical for these two choices of j_n^π. Although certain types of defects in the component calculations can be compensated by changing the degree of j-mixing, it is likely that distorted-wave calculations using the adiabatic deuteron potential adequately describe this transition, and that both values of j_n^π contribute significantly.

The spectroscopic factors obtained by comparing the present data with distorted-wave calculations are shown in table 2. Although there are large differences among the values obtained using deuteron potentials A, B, and D, the results with potential D (the adiabatic potential), are in reasonable agreement with the results of ref. [45]), except for the 0.159 and 0.317 MeV states. The D-state of the deuteron has essentially no effect on the magnitude of the cross section at angles near the stripping peak, as shown in fig. 9, and therefore does not affect the spectroscopic factors in table 2.

TABLE 2

Spectroscopic factors for states in ^{117}Sn

E_x (MeV)	Potential A (global analysis [25]))	Potential B (elastic scattering)	Potential D (adiabatic)	Carson and McIntyre (ref. [45]))
0.0	0.90	0.51	0.45	0.52
0.159	0.87	1.08	0.54	0.76
0.317	0.62	0.88	0.48	0.79
1.020	0.10	0.094	0.058	0.064
1.179	0.059	0.053	0.034	0.039
1.308	0.034	0.063	0.030	0.037

7. Comparison of DWBA calculations using various deuteron potentials

The results presented in the last section showed that traditional DWBA calculations, in which the optical potentials are taken to be those which reproduce the relevant elastic scattering data, do not reproduce the (d, p) data in the present experiment. The difficulty experienced in reproducing the (d, d) data suggests that the difficulties probably lie with the deuteron, rather than with the proton potential. This conjecture is supported by the fact that the agreement with the data is greatly improved by using an adiabatic deuteron potential, without alterations to the proton potential. The success of the adiabatic potential is particularly interesting not only because this potential has been constructed in a physically reasonable way from nucleon potentials, without adjustable parameters, but also because the energy in the present experiment is

much lower than the energies at which adiabatic potentials are usually employed (20 MeV or above) [10,41,47-49]). As the energy is lowered the basic adiabatic assumption, that the motion of the deuteron's c.m. is more rapid than its internal motion, becomes less valid.

The lack of agreement between the reaction data and DWBA calculations using the elastic scattering deuteron potential B could arise in several ways. The first possibility is that this potential is unphysical, and that there exists a second potential which describes both the elastic scattering and the reaction data. Although the existence of an alternative potential cannot be ruled out, the large amount of effort expended in searching for potentials which reproduce the elastic scattering data makes it unlikely that such a potential has been overlooked.

The second possibility is that the DWBA method itself is inadequate. In particular, the success of the adiabatic potential suggests that the three-body effects which are neglected in the traditional DWBA method are significant.

A third possible origin for the discrepancies between the reaction data and the corresponding calculations is the choice of the functional form of the optical potential. All of the calculations which are described in this paper were performed with optical potentials containing a Woods-Saxon radial dependence. At energies near the Coulomb barrier, the interaction between the nucleus and the incoming deuteron may be unusually sensitive to the details of the shape of the potential near the nuclear surface, and a Woods-Saxon shape may be inadequate in the surface region. It would be particularly interesting to see whether the use of a potential with a different radial dependence in the surface region could improve the description of both the reaction and (d, d) data presented here, as well as other (d, d) analyzing power measurements at energies near the Coulomb barrier.

Comparison of the fits to the (d, p) data obtained with the global and adiabatic potentials (see figs. 2, 7, and 8) reveals that the adiabatic potential gives better overall agreement for the $l_n = 0$ and $l_n = 2$ transitions (figs. 2 and 7) than does the global potential, while the global potential leads to more satisfactory results for the $l_n = 3$ and $l_n = 5$ transitions (fig. 8). The superiority of the global potential for higher l-values is most pronounced at forward reaction angles, and is particularly evident in the case of the transition to the 0.317 MeV state. Roughly speaking, small reaction angles and large values of l_n are associated with large impact parameters, and reactions with these characteristics are therefore sensitive to the asymptotic behavior of the wave functions. Elastic scattering is also most sensitive to the asymptotic behavior of the wave functions, so it is not surprising that the superiority of the global phenomenological potential is most apparent for large values of l_n and small reaction angles. The adiabatic potential, on the other hand, appears to be more successful in circumstances which involve deeper penetration into the nuclear interior.

8. Conclusions

We have presented cross section and vector analyzing power data for the ^{116}Sn $(\vec{d}, p)^{117}$Sn reaction leading to six states in ^{117}Sn, as well as for the elastic scattering of the particles in the entrance and exit channels in the (d, p) reaction. In addition, we have measured the proton polarization for the $l_n = 0$ ground state transition. The existence of cross section, vector analyzing power, and proton polarization measurements for the ground state transition makes this a particularly useful set of data for comparison with theory.

The results of our optical-model analysis of the proton elastic scattering data were consistent with previous work, but the deuteron elastic scattering data could not be reproduced using an optical potential with conventional parameters. In particular, conventional deuteron potentials failed to reproduce the predominantly negative trend of the analyzing power data. Satisfactory agreement with the (d, d) measurements was obtained using a potential which included a spin-orbit potential obtained from the folding model and a real central potential characterized by unconventional values of V_0 and a_0. However, the (d, p) results were poorly described by DWBA calculations in which this deuteron potential was used. Although the existence of other deuteron potentials which describe both the (d, d) and (d, p) data cannot be ruled out, the considerable effort which was required to obtain reasonable agreement between the (d, d) data and the corresponding calculations leads us to believe that this is probably not the case. In addition, the relative success of the deuteron potential obtained from the adiabatic prescription may indicate that three-body effects cause the failure of the traditional DWBA prescription in the present case.

Johnson's method for the separation of proton and deuteron spin-dependent effects has been applied to our data for the $l_n = 0$ ground state transition. The results of this analysis indicated that the small observed analyzing power is the result of considerable cancellation of the contribution from the proton spin-orbit potential by the contribution from the deuteron spin-orbit potential. This cancellation makes the analyzing power sensitive to small changes in either contribution, and may be responsible, at least in part, for the difficulty sometimes encountered in describing the analyzing power in $l_n = 0$ reactions with distorted-wave calculations.

The spins and spectroscopic factors obtained in the analysis of our data for transitions to excited states were generally in agreement with previous work. In the case of the 1.497 MeV state in ^{117}Sn, however, our $j^\pi = \frac{3}{2}^+$ assignment is in conflict with an earlier tentative result. Distorted-wave calculations for the transitions to excited states indicated that the data for $l_n = 0$ and $l_n = 2$ transfers were best reproduced using the adiabatic deuteron potential, while a global phenomenological potential gave better results for the $l_n = 3$ and $l_n = 5$ transfers.

The authors wish to thank R. C. Johnson for many helpful discussions, particularly regarding the adiabatic prescription and the separation of proton and deuteron spin-dependent effects.

References

1) L. J. B. Goldfarb, Third Int. Symp. on polarization phenomena in nuclear reactions, ed. H. H. Barschall and W. Haeberli (University of Wisconsin Press, 1971) p. 205
2) L. J. B. Goldfarb and R. C. Johnson, Nucl. Phys. **18** (1960) 353
3) R. C. Johnson, Nucl. Phys. **A90** (1967) 289
4) R. R. Cadmus and W. Haeberli, to be published
5) T. J. Yule and W. Haeberli, Phys. Rev. Lett. **19** (1967) 756
6) T. J. Yule and W. Haeberli, Nucl. Phys. **A117** (1968) 1
7) R. C. Johnson, Nucl. Phys. **35** (1962) 654
8) R. D. Rathmell, P. J. Bjorkholm and W. Haeberli, Nucl. Phys. **A206** (1973) 459
9) L. S. Michelman, S. Fiarman, E. J. Ludwig and A. B. Robbins, Phys. Rev. **180** (1969) 1114
10) R. C. Johnson and P. J. R. Soper, Phys. Rev. **C1** (1970) 976
11) G. R. Satchler, Nucl. Phys. **8** (1958) 65
12) L. C. Biedenharn, Nucl. Phys. **10** (1959) 620
13) T. B. Clegg, G. A. Bissinger, W. Haeberli and P. A. Quin, Third Int. Symp. on polarization phenomena in nuclear reactions, ed. H. H. Barschall and W. Haeberli (University of Wisconsin Press, 1971) p. 835
14) S. E. Vigdor, R. D. Rathmell, H. S. Liers and W. Haeberli, Nucl. Phys. **A210** (1973) 70
15) N. Rohrig and W. Haeberli, Nucl. Phys. **A206** (1973) 225
16) R. R. Cadmus, Jr. and W. Haeberli, Nucl. Instr. **129** (1975) 403
17) J. V. Tyler, Ph.D. thesis, University of Wisconsin, 1973, available from University Microfilms, Ann Arbor, Michigan
18) P. Schwandt, T. B. Clegg and W. Haeberli, Nucl. Phys. **A163** (1971) 432
19) P. Schwandt and W. Haeberli, Nucl. Phys. **A110** (1968) 585
20) D. C. Kocher and W. Haeberli, Nucl. Phys. **A172** (1971) 652
21) W. Haeberli, in Nuclear spectroscopy and reactions, Part A, ed. J. Cerny (Academic Press, New York, 1974) p. 151
22) R. G. Seyler and L. J. B. Goldfarb, Third Int. Symp. on polarization phenomena in nuclear reactions, ed. H. H. Barschall and W. Haeberli (University of Wisconsin Press, 1971) p. 779
23) M. B. Hooper, Nucl. Phys. **76** (1966) 449
24) J. A. R. Griffith, M. Irshad, O. Karban and S. Roman, Nucl. Phys. **A146** (1970) 193; **A166** (1971) 675
25) J. M. Lohr and W. Haeberli, Nucl. Phys. **A232** (1974) 381
26) S. E. Vigdor and W. Haeberli, Nucl. Phys. **A253** (1975) 55
27) L. S. Rodberg, Nucl. Phys. **15** (1960) 72
28) F. D. Becchetti, Jr. and G. W. Greenlees, Phys. Rev. **182** (1969) 1190
29) P. Schwandt, University of Indiana, unpublished
30) J. D. Childs, W. W. Daehnick and M. J. Spisak, Phys. Rev. **C10** (1974) 217
31) J. D. Childs, Ph.D. thesis, University of Pittsburgh (1976) available from University Microfilms, Ann Arbor, Michigan
32) L. D. Knutson and W. Haeberli, Phys. Rev. **C12** (1975) 1469
33) S. Watanabe, Nucl. Phys. **8** (1958) 484
34) F. G. Perey and G. R. Satchler, Nucl. Phys. **A97** (1967) 515
35) B. A. Robson, Oak Ridge Nat. Lab. report ORNL-TM-1831 (1967) available from the Division of Technical Information, Oak Ridge, Tennessee
36) G. R. Satchler, Nucl. Phys. **21** (1960) 116
37) J. M. Lohr, Ph.D. thesis, University of Wisconsin, 1972, available from University Microfilms, Ann Arbor, Michigan
38) J. D. Harvey and F. D. Santos, University of Surrey, unpublished
39) R. C. Johnson and F. D. Santos, Part. and Nucl. **2** (1971) 285
40) C. M. Perey and F. G. Perey, Phys. Rev. **132** (1963) 755
41) J. D. Harvey and R. C. Johnson, Phys. Rev. **C3** (1971) 636
42) G. C. Madueme, L. O. Edvardson and L. Westerberg, Phys. Scripta **13** (1976) 17
43) D. B. Beery, G. Berzins, W. B. Chaffee, W. H. Kelly and W. C. McHarris, Nucl. Phys. **A123** (1969) 649
44) E. J. Schneid, A. Prakash and B. L. Cohen, Phys. Rev. **156** (1967) 1316
45) P. L. Carson and L. C. McIntyre, Jr., Nucl. Phys. **A198** (1972) 289
46) K. Way *et al.*, Nucl. Data Sheets 1959–1965 (Academic Press, New York, 1966) p. 967
47) G. R. Satchler, Phys. Rev. **C4** (1971) 1485
48) G. H. Rawitscher, Phys. Rev. **C11** (1975) 1152
49) G. L. Wales and R. C. Johnson, Nucl. Phys. **A274** (1976) 168